Biochimica et Biophysica Acta 1837 (2014) 1019–1026

Contents lists available at ScienceDirect

Biochimica et Biophysica Acta

journal homepage: www.elsevier.com/locate/bbabio

Characterization of quinol-dependent nitric oxide reductase from *Geobacillus stearothermophilus*: Enzymatic activity and active site structure ☆

Erina Terasaka [a,b], Norihiro Okada [a,b], Nozomi Sato [a,c], Yoshihiko Sako [c], Yoshitsugu Shiro [a,b,*], Takehiko Tosha [a,**]

[a] RIKEN SPring-8 Center, Kouto, Sayo, Hyogo 679-5148, Japan
[b] Graduate School of Life Science, University of Hyogo, Hyogo 678-1297, Japan
[c] Division of Applied Biosciences, Graduate School of Agriculture, Kyoto University, Kyoto 606-8502, Japan

ARTICLE INFO

Article history:
Received 21 November 2013
Received in revised form 10 February 2014
Accepted 15 February 2014
Available online 22 February 2014

Keywords:
Nitric oxide reductase
Heme
Non-heme metal
Cytochrome *c* oxidase
Resonance Raman
Proton transfer

ABSTRACT

Nitric oxide reductase (NOR) catalyzes the reduction of nitric oxide to generate nitrous oxide. We recently reported on the crystal structure of a quinol-dependent NOR (qNOR) from *Geobacillus stearothermophilus* [Y. Matsumoto, T. Tosha, A.V. Pisliakov, T. Hino, H. Sugimoto, S. Nagano, Y. Sugita and Y. Shiro, *Nat. Struct. Mol. Biol.* 19 (2012) 238–246], and suggested that a water channel from the cytoplasm, which is not observed in cytochrome *c*-dependent NOR (cNOR), functions as a pathway transferring catalytic protons. Here, we further investigated the functional and structural properties of qNOR, and compared the findings with those for cNOR. The pH optimum for the enzymatic reaction of qNOR was in the alkaline range, whereas *Pseudomonas aeruginosa* cNOR showed a higher activity at an acidic pH. The considerably slower reduction rate, and a correlation of the pH dependence for enzymatic activity and the reduction rate suggest that the reduction process is the rate-determining step for the NO reduction by qNOR, while the reduction rate for cNOR was very fast and therefore is unlikely to be the rate-determining step. A close examination of the heme/non-heme iron binuclear center by resonance Raman spectroscopy indicated that qNOR has a more polar environment at the binuclear center compared with cNOR. It is plausible that a water channel enhances the accessibility of the active site to solvent water, creating a more polar environment in qNOR. This structural feature could control certain properties of the active site, such as redox potential, which could explain the different catalytic properties of the two NORs. This article is part of a Special Issue entitled: 18th European Bioenergetic Conference.

1. Introduction

Microbial denitrification, in which nitrate (NO_3^-) is stepwise reduced to dinitrogen (N_2) through nitrite (NO_2^-), nitric oxide (NO) and nitrous oxide (N_2O), is an example of anaerobic respiration. Some soil bacteria can produce bio-energy, such as ATP, by denitrification. Nitric oxide reductase (NOR) is a membrane-integrated metalloprotein, which, as a part of the denitrification process, catalyzes the reduction of NO to N_2O by the use of two protons and two electrons ($2NO + 2H^+ + 2e^- \rightarrow N_2O + H_2O$). This reaction involves the important chemical process of N–N bond formation in the global nitrogen cycle, thus enabling the eventual release of N_2 into the atmosphere. NOR is also an attractive target of study in Earth science, as N_2O, the product of the NOR-catalyzed reaction, is both an ozone (O_3) depleting substance and a greenhouse gas with 310 times potency of carbon dioxide (CO_2) [1].

On the basis of similarities in the amino acid sequence, NOR has been thought to share the same ancestor protein with aerobic terminal oxidases such as cytochrome *c* oxidase (CcO) [2–4]. CcO catalyzes the reduction of O_2 to water by four protons and four electrons ($O_2 + 4H^+ + 4e^- \rightarrow 2H_2O$) at a heme iron and copper (Cu_B) binuclear center, and, coupled with the catalytic reaction, pumps protons across the membrane. The generated electrochemical proton gradient is then used for ATP synthesis. High resolution crystal structures, along with extensive biochemical and biophysical studies of CcOs provide a detailed picture of the mechanism involved in the proton pumping in a process coupled with the O_2 reduction reaction [5–7]. Since NOR exhibits NO reduction activity without proton pumping, a knowledge of the structural characteristics of NOR is crucial for elucidating functional conversion – for example, substrate selectivity and proton pumping ability – of these respiratory enzymes during molecular evolution.

Abbreviations: NOR, bacterial nitric oxide reductase; qNOR, quinol-dependent NOR; cNOR, cytochrome *c*-dependent NOR; CcO, cytochrome *c* oxidase; DDM, *n*-dodecyl-β-D-maltoside; OG, *n*-octyl-β-D-glucoside; PMS, phenazine methosulfate.

☆ This article is part of a Special Issue entitled: 18th European Bioenergetic Conference.

* Correspondence to: Y. Shiro, RIKEN SPring-8 Center, 1-1-1 Kouto, Sayo, Hyogo 679-5148, Japan. Tel.: +81 791 58 2817.
** Corresponding author. Tel.: +81 791 58 2817.
E-mail addresses: yshiro@riken.jp (Y. Shiro), ttosha@spring8.or.jp (T. Tosha).

http://dx.doi.org/10.1016/j.bbabio.2014.02.017
0005-2728/

Three classes of NOR have been identified in bacteria and archaea. The first class, called cNOR, is a two subunit enzyme that is observed only in denitrifying bacteria, and uses soluble proteinous electron donors, such as cytochrome *c*, for the catalytic reaction [8]. The second class, known as quinol-dependent NOR (qNOR), is a single-subunit enzyme that is observed in non-denitrifying pathogenic bacteria as well as in denitrifying bacteria and archaea [8–10]. The physiological role of qNOR of pathogenic bacteria is to detoxify NO produced by the immune system of the host [11,12]. qCu$_A$NOR which was isolated from denitrifying *Bacillus azotoformans* and has di-copper site at the hydrophilic domain represents the third class [13], although little is known regarding this enzyme, with not even sequence information available. Of these NOR enzymes, cNOR is the most extensively studied [14–17]. We published the first crystal structure of NOR, cNOR from *Pseudomonas aeruginosa* in 2010 [18]. The NO reduction site consists of a heme (designated as heme b_3) iron and a non-heme iron (Fe$_B$), and is structurally related to the heme/Cu$_B$ binuclear center in CcO. Fe$_B$ has a distorted trigonal–bipyramidal geometry with three histidine ligands and one glutamate ligand. From the *P. aeruginosa* cNOR structure and structure-based molecular dynamics simulation, no evidence for the existence of a proton pumping pathway was found, but potential pathways for transferring catalytic protons from the periplasmic side were identified [18,19]. Overall, this is consistent with the non-electrogenicity of the NO reduction reaction catalyzed by cNOR [17,20].

We have also recently reported the crystal structure of *Geobacillus stearothermophilus* qNOR [21]. Compared with *P. aeruginosa* cNOR, the overall structure of *G. stearothermophilus* qNOR is similar, but no obvious proton transfer pathway from the extracellular side was found. Instead, a water-filled hydrophilic channel from the cytoplasmic side to the binuclear center was observed. Structure-based mutagenesis and molecular dynamics simulation studies suggested that the water channel could possibly function as a proton transfer pathway for the catalytic reaction. This finding for *G. stearothermophilus* qNOR is very surprising, as, in two NOR enzymes performing the same enzymatic reaction, catalytic protons seem to be supplied to the active site from differing directions.

However, no supporting data is available for this novel finding. Only a few structural and functional studies on qNORs have been reported so far [22–24], and, as a result, the functional properties of qNOR are poorly understood as compared with the well-studied cNOR. In addition (and unfortunately), our *G. stearothermophilus* qNOR expressed in *Escherichia coli* and purified using *n*-dodecyl-β-D-maltoside (DDM) as a detergent was isolated as a mixture of active and inactive forms in a ratio of about 3:7. Atomic absorption analysis showed that in the active enzyme, a non-heme iron, Fe$_B$, is present at the binuclear active center, as in the case of *P. aeruginosa* cNOR, whereas, in the inactive form, the Fe$_B$ had accidentally been replaced by Zn (Zn$_B$) [21]. In an attempt to improve the final yield of the active enzyme, more supplementary iron was used in expression cultures, and alternative detergents applied in the purification procedure; however, the purified sample still resulted in a similar population (~70%) of the inactive Zn$_B$-bound qNOR. When using *n*-octyl-β-D-glucoside (OG) as a detergent (for crystallization purposes), the active Fe$_B$-bound form was precipitated, leaving only the inactive Zn$_B$ form to be crystallized [21]. Our crystal structure of *G. stearothermophilus* qNOR was thus that of an inactive Zn$_B$ form. Therefore, we now report on the characterization of the active Fe$_B$ form of *G. stearothermophilus* qNOR in this study. We examined the catalytic properties, in particular the proton uptake mechanism, of *G. stearothermophilus* qNOR by measuring the enzymatic activity under different pH values, because the proton transfer pathway would be expected to be different between *G. stearothermophilus* qNOR and cNOR on the basis of their structural comparison [18,19,21]. In addition to functional properties, the structure of the heme environment of *G. stearothermophilus* qNOR was characterized by resonance Raman spectroscopy, in an attempt to elucidate structure–function relationships. A comparison of findings for *G. stearothermophilus* qNOR with those for *P. aeruginosa* cNOR permits the structural and functional differences in these two classes of NOR to be determined and discussed.

2. Materials and methods

2.1. Sample preparation

The expression and purification of *G. stearothermophilus* qNOR followed a previous method [21]. Briefly, pET-22 plasmid encoding qNOR with a C-terminal His-tag was transformed into an *E. coli* Rosetta 2 DE3 (Novagen) strain. The *E. coli* was grown in 2xTY media with $FeSO_4$ and δ-aminolevulinic acid, with expression of qNOR induced by IPTG. The harvested cells were lysed, and the membrane fraction was isolated. After solubilization in 2% Triton X-100, the solubilized fraction was loaded onto a Ni-NTA column. The column was washed with buffer containing 0.05% DDM (Dojindo) or 1% OG (Dojindo) to exchange the detergent. The qNOR fraction was eluted with 300 mM imidazole, and then further purified using a Superdex 200 column. Fractions with $A_{Soret}/A_{280} > 0.7$ were employed in further experiments. The concentration of the purified sample was determined using a molar extinction coefficient of 206 mM^{-1} cm^{-1} at the Soret peak. Analysis of metal content by inductively coupled plasma atomic emission spectroscopy showed a complete occupation of zinc at the non-heme metal site with OG as the detergent, whereas the non-heme metal site was occupied by either iron (~30%) or zinc (~70%) when DDM was used [21]. Because the sample with zinc at the non-heme metal site was enzymatically inactive, qNOR prepared with OG was used only for spectroscopic characterization of the active site, [21]. The purified sample was stored at −80 °C until use.

The cNOR used in this study was purified from anaerobically cultured *P. aeruginosa*. Preparation of membranes and purification of cNOR were performed as previously described [18]. The purified fractions with $A_{Soret}/A_{280} > 1.5$ were used in further experiments. The concentration of the purified sample was determined using the molar extinction coefficient of 300 mM^{-1} cm^{-1} at the Soret peak [18]. The sample was stored at −80 °C until use.

2.2. NO reduction activity measurements

NO reduction activity was measured using a Clark-type electrode equipped with an ISO-NO mark II system (WPI). The anaerobic assay mixture (0.9 mL) consisted of 50 mM Tris buffer (pH 7.0), 0.05% DDM, 100 mM D-glucose, 10 μg/mL glucose oxidase, and 10 μg/mL catalase. For the pH dependence measurements, Bis-Tris, Tris and CAPS buffers were used for pH 6.0, 7.0–9.0, and 10.0, respectively. As an electron transfer system, 1 mM sodium ascorbate and 100 μM phenazine methosulfate (PMS) were used. NO saturated buffer was added to a final concentration of 10–40 μM. Once a stable electrode response was observed, the addition of NOR (final concentration: 0.2–0.5 μM) initiated the NO reduction reaction. NO reduction rates were calculated from the difference in the slope of the activity trace before and after the addition of the enzyme. Although substrate inhibition was reported in cNOR from *Paracoccus denitrificans* [25], substrate inhibition was not observed under the current assay condition. For qNOR, the activity was estimated relative to the Fe$_B$-containing active enzyme (30% of total enzyme). The measurements were carried out at 40 °C (for qNOR) or 20 °C (for cNOR). The NO reduction rates were measured at different pH values, ranging from pH 6.0 to 10.0 (the ascorbate/PMS electron transfer system does not function effectively at a pH of less than 5.0), and determined from at least three independent measurements.

2.3. Stopped flow measurements

The reduction of the qNOR or cNOR by the ascorbate/PMS electron transfer system was monitored by a rapid-scanning system equipped with a stopped flow apparatus (Unisoku, RSP-1000) at

ambient temperature in 50 mM Bis-Tris buffer (pH 6.0) or 50 mM Tris buffer (pH 9.0) containing 0.05% DDM under anaerobic conditions. The anaerobically prepared assay solution containing 4 μM of as-isolated (resting oxidized) form of NOR, in which all iron atoms are in ferric state, was transferred to one of the stopped-flow reservoirs. The other reservoir was filled with the anaerobically prepared solution containing 2 mM sodium ascorbate and 10 μM PMS. The reaction was initiated by mixing the two solutions and followed by monitoring the spectral change. To compare the rapid-scanning spectrum with that of the oxidized or reduced sample, the UV/vis absorption spectra of NORs were recorded on a U-3010 spectrometer (Hitachi).

2.4. Resonance Raman measurements

Resonance Raman spectra for reduced CO-bound forms of detergent solubilized NORs were obtained with a single polychromator (Jovin Yvon, SPEX750M) equipped with a liquid nitrogen-cooled CCD detector (Roper Scientific, Spec 10:400B/LN). Reduced CO-bound NORs were produced by adding an excess amount of dithionite solution under CO or isotopic ^{13}CO (SI Science) atmosphere. The formation of the reduced CO-bound form was confirmed by a UV/vis absorption spectrum recorded on a U-3310 spectrometer (Hitachi). The 413.1 nm line from a Kr ion laser (Spectra Physics, model BeamLok 2060) was used for the excitation. The laser power was adjusted to ~0.1 mW at the sample point to avoid photo dissociation of the CO ligand. Raman shifts were calibrated against indene, acetone and aqueous solution of ferrocyanide. The measurements were performed with a spinning cell (~2000 rpm) for sample concentrations of 20–40 μM.

3. Results

3.1. pH dependence of NO reduction activity of NORs

Since the NOR-catalyzed reaction requires two protons, we examined the effects of pH on the NO reduction activity to obtain insights into the mechanism of reduction of NO by NOR. For the measurement of *G. stearothermophilus* qNOR, DDM-solubilized sample was used, in which the *ca.* 30% Fe_B-contained active enzyme of a Fe_B/Zn_B-qNOR mixture gives a catalytic NO consumption. In the pH range from pH 4.0 to 10.0, the UV/vis absorption spectra for qNOR were nearly identical (data not shown), confirming that the enzyme is stable over this pH range. When measured with the ascorbate/PMS electron transfer system and 40 μM NO at pH 7.0 at 40 °C, qNOR showed a steady-state NO consumption of ~60 μM-NO min^{-1} per μM of Fe_B-containing active enzyme (~20 μM-NO min^{-1} per μM of total enzyme including Zn_B-bound inactive form) (Fig. 1), which is consistent with a previously reported value [21]. Fig. 1 displays the rates of NO consumption by qNOR for solutions of varied pH values. These findings show that the consumption of NO was an order of magnitude faster under alkaline conditions (pH 9.0 and 10.0) compared to acidic conditions (pH 6.0), while the optimum growth pH of *G. stearothermophilus* is 6.0–7.0 [26]. Currently, the reason why the optimum pH for the catalytic NO reduction activity in the purified enzyme differs from that of the bacterial growth is unclear.

The NO reduction activity and the pH dependence of qNOR were compared with those of *P. aeruginosa* cNOR. The rate of consumption of NO for qNOR was considerably slower than that of cNOR at 20 °C (Fig. 1), presumably due to the disparity between the temperature for the activity measurement (40 °C) and that required for optimum growth of thermophilic *G. stearothermophilus* (~55 °C). A similar observation was also reported for the case of the cNOR of *Thermus thermophilus* [27]. Another reason for the low NO reduction activity compared to cNOR is that qNOR does not have heme *c* in the hydrophilic domain. It might indicate that we still have not found an optimal reduction system for the qNOR compared to the heme *c*-containing cNORs that react well with ascorbate/PMS. In addition, it was found that the

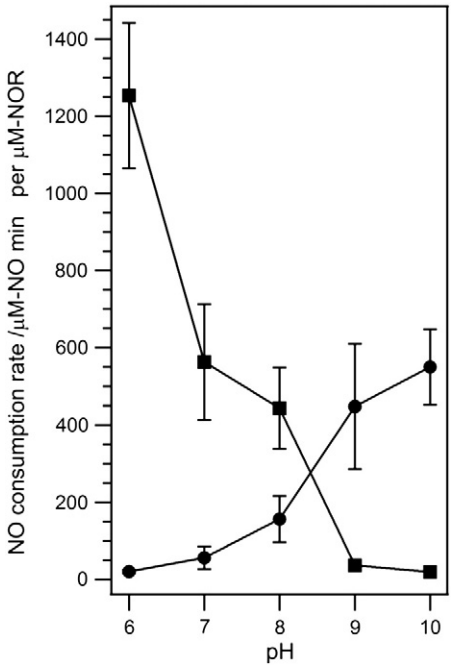

Fig. 1. pH dependence of the NO reduction activity in *G. stearothermophilus* qNOR (*closed circles*) and *P. aeruginosa* cNOR (*closed squares*). The NO reduction activity in qNOR is per Fe_B-contained active enzyme. The NO consumption rates were obtained at 40 μM of NO. Details of the other condition for the activity measurements are shown in "Materials and methods". Error bars represent the standard deviation calculated from at least three independent experiments.

pH dependence of the catalytic NO reduction is in sharp contrast between the two NORs; with cNOR more active under acidic conditions (pH 6.0) than under alkaline conditions (pH 9.0), as seen in Fig. 1. Such a marked difference in pH dependence suggests that the mechanism of the catalytic NO reduction is different between qNOR and cNOR. It is pertinent here to note that a difference in catalytic mechanism between qNOR and cNOR was also suggested by a study on proton uptake; namely that the pH dependence of the reaction between fully reduced qNOR and oxygen molecule differs from the corresponding reaction using cNOR from *Pa. denitrificans* [24].

3.2. Rate of reduction of redox centers in NORs

To support our above hypothesis, we focused on the reduction of the redox centers, from considering that the NOR reaction requires electrons as well as protons. Upon mixing qNOR with a reducing agent (ascorbate/PMS) at pH 6.0 or pH 9.0 using a stopped-flow rapid scan instrument, a change in the visible absorption spectrum was observed in the case of qNOR (Fig. 2A). The spectrum of qNOR after mixing with ascorbate/PMS did not reach that of fully (100%) reduced qNOR, which can be produced by the addition of dithionite, $Na_2S_2O_4$. In the case of qNOR, reduction can be extremely slow. In contrast to the well-studied *Pa. denitrificans* cNOR, in which ferric heme b_3 adopts high spin state and exhibits a charge transfer band around 600 nm [25,28], there was no corresponding peak in the visible absorption spectrum of oxidized qNOR. Consistent with this, we could not detect any Raman signals assignable to high spin heme in the resonance Raman spectrum for oxidized qNOR (data not shown). Therefore, we could not discriminate two hemes, heme *b* and heme b_3, and so could not fully characterize the state of the ascorbate/PMS-reduced qNOR. In simply comparing the rate of reduction, the initial rates of the reaction were obtained at different pH values from a time course for spectral changes at 423 nm, the absorption maximum of the fully reduced state. As shown in Fig. 2B, the initial reduction rate obtained for qNOR at pH 9.0 (2.3 $\Delta Abs_{423\ nm}/s$) was faster than that at pH 6.0 (0.93 $\Delta Abs_{423\ nm}/s$),

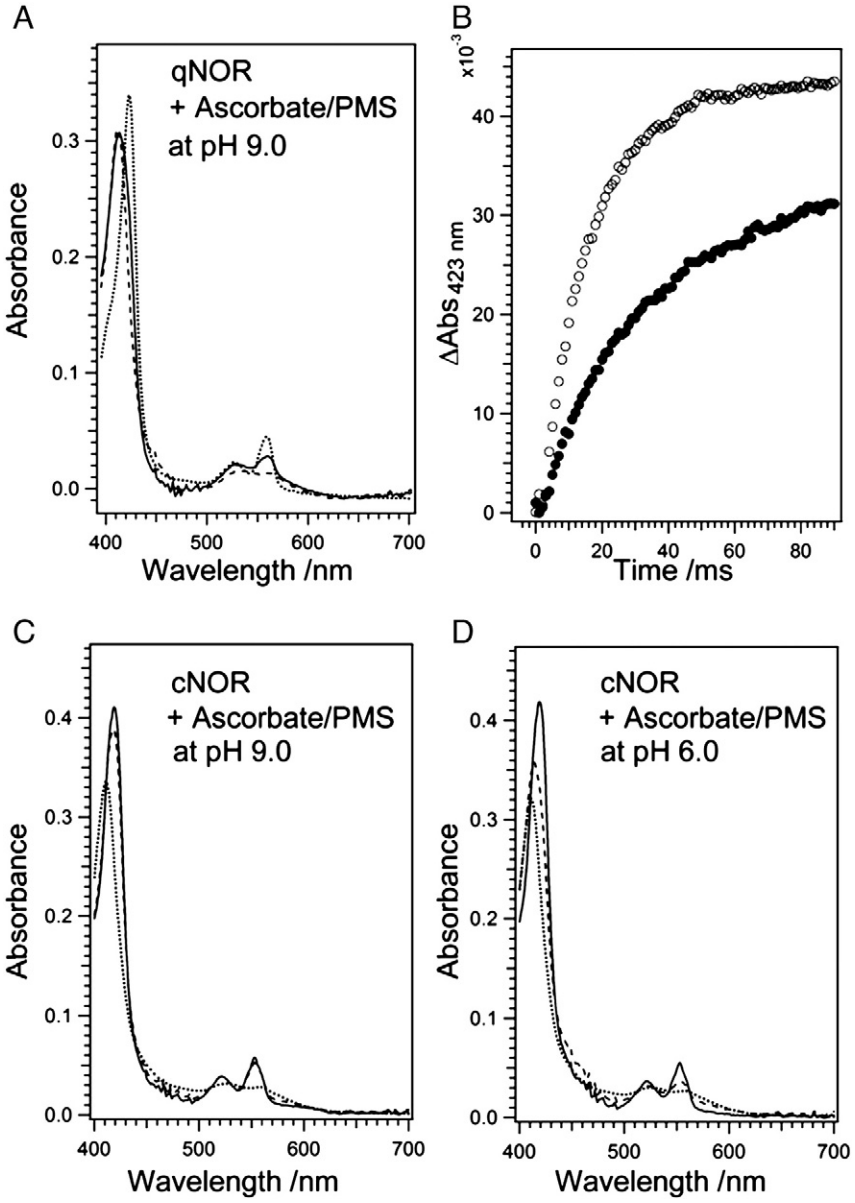

Fig. 2. Reduction of NORs by an ascorbate/PMS electron transfer system. Panel A displays visible absorption spectra obtained 5 ms (*broken curve*) and 1 s (*solid curve*) after mixing qNOR and the reducing agent at pH 9.0. The spectrum for the fully reduced state prepared by the addition of dithionite is also shown as a reference (*dotted curve*). Panel B displays the time courses for the absorbance at 423 nm after mixing qNOR and the reducing agent at pH 9.0 (*open circles*) and pH 6.0 (*closed squares*). Panels C and D display visible absorption spectra after mixing cNOR and the reducing agent at pH 9.0 and pH 6.0, respectively. The traces shown are 5 ms (*broken curve*) and 1 s (*solid curve*) after mixing cNOR and the reductant. *Dotted curve* represents the absorption spectrum for fully oxidized cNOR for comparison.

and thereby consistent with the dependence of NO reduction activity on pH.

In contrast to the relatively slow reduction rate of qNOR, reduction of the redox centers for cNOR by ascorbate/PMS was too fast to permit observation by a stopped-flow technique, i.e., about ~80% of hemes (heme *c*, heme *b* and heme b_3) in cNOR were already reduced within the mixing dead time (~5 ms) in cNOR at pH 9.0, as shown in Fig. 2C; indicating that cNOR is much more readily reduced than qNOR. In addition, it is also noteworthy that, at pH 6.0, ~40% of cNOR was reduced within the mixing dead time (Fig. 2D), with the reduction rate apparently slower at pH 6.0 than at pH 9.0. On the basis of the shape of the spectral changes, all types of hemes (heme *c*, heme *b* and heme b_3), not only a particular heme, were reduced at pH 6.0. From these observations, it is likely that the reduction of the redox centers is the rate-determining step in the catalytic reaction for qNOR, but not in the cNOR reaction. While previous studies reported rate constants for several steps in the reaction by cNOR of *Pa. denitrificans* [29–31], further study is required to elucidate the rate-determining step of the reaction catalyzed by cNOR.

3.3. Resonance Raman characterization of active site structures of NORs

To understand the structural origin responsible for the different functional properties between *G. stearothermophilus* qNOR and *P. aeruginosa* cNOR, we characterized the active site structures of the proteins by resonance Raman spectroscopy. The CO-associated vibrations in the reduced CO-bound form, in which the active site heme b_3 iron is coordinated by CO, are sensitive to the heme environment, and are a useful probe for examining the structural properties of the active site [32,33]. Fig. 3 displays the resonance Raman spectra for CO-bound *G. stearothermophilus* qNOR at pH 9.0 and 6.0. The spectra were indistinguishable, indicating that the active site structure is insensitive to pH change. For the qNOR containing a Fe_B and Zn_B mixture at the non-heme metal site (Fe_B/Zn_B-qNOR), the difference spectrum obtained

from the isotope substitution for CO indicates that the Raman lines at 481, 495, 577 and 1962 cm^{-1} are derived from vibrational modes that include the heme Fe – CO unit. Through comparison of Raman data for other heme proteins [33,34], the Raman lines at 577 and 1962 cm^{-1} are assignable to δ_{FeCO} and ν_{C-O}, respectively. The Raman lines at 481 and 495 cm^{-1} can be assigned to ν_{Fe-CO}, indicating that the Fe – CO moiety has two conformations in the Fe_B/Zn_B-qNOR. The presence of two conformations of the Fe – CO moiety could be due to the mixture of Fe_B and Zn_B at the non-heme metal site.

To distinguish the Raman signals arising from qNOR with Zn_B at the non-heme metal site from those for the sample with Fe_B, we collected the resonance Raman spectra for the qNOR sample prepared using OG as a detergent, in which the non-heme metal site is occupied only by Zn_B (Zn_B-qNOR). As shown in Fig. 3, for the case of Zn_B-qNOR, δ_{FeCO} and ν_{C-O} are observed at 577 and 1962 cm^{-1}, which are nearly identical to those for the Fe_B/Zn_B-qNOR. On the other hand, a single prominent ν_{Fe-CO} peak was detected at 481 cm^{-1} in the Zn_B-qNOR, whereas two ν_{Fe-CO} peaks were observed at 481 and 495 cm^{-1} in the Fe_B/Zn_B qNOR. In addition to the ν_{Fe-CO} peak at 481 cm^{-1}, a minor ν_{Fe-CO} line was observed at 525 cm^{-1} in the Zn_B-qNOR (Fig. 3). The ν_{Fe-CO} mode at 525 cm^{-1} is assignable to 5-coordinated heme-CO species. This species was not detected in the mixture of Fe_B- and Zn_B-qNOR, possibly due to the low population of 5-coordinated heme-CO species only observed in Zn_B-qNOR, not in Fe_B-qNOR. Thus, we reasonably assigned the Raman line at 495 cm^{-1} to the ν_{Fe-CO} for the active form of Fe_B-qNOR.

For cNOR, three isotope-sensitive Raman lines were detected at 477, 568 and 1972 cm^{-1} in the CO-bound form (Fig. 4), which are assignable to ν_{Fe-CO}, δ_{FeCO} and ν_{C-O}, respectively (Table 1). Similar to qNOR, these Raman lines were insensitive to pH, as evidenced by the fact that no spectral difference was observed at pH 9.0 and 6.0 (Fig. 4). The frequencies for the vibrational modes including the Fe – CO moiety in cNOR are quite similar to those reported for *Pa. denitrificans* cNOR; ν_{Fe-CO}, δ_{FeCO} and ν_{C-O} peaks were observed at 478, 570, and 1970 cm^{-1}, respectively [34], but not to those of qNOR (Table 1). Such an observation indicates that the active site structures in solution are different between qNOR and cNOR, which indicates that these two types of NORs have quite different functional properties.

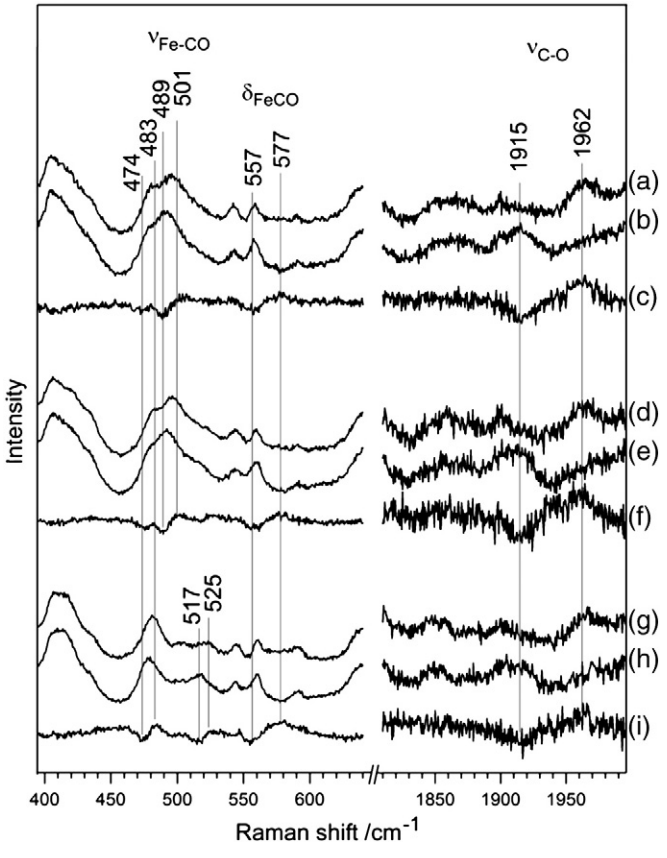

Fig. 3. Resonance Raman spectra of the reduced CO-bound qNOR from *G. stearothermophilus* with excitation at 413.1 nm. Traces shown were obtained from CO-bound Fe/Zn-qNOR (a), ^{13}CO-bound Fe/Zn-qNOR (b), and the difference (CO–^{13}CO) (c) at pH 9.0, and those at pH 6.0; (d), (e) and (f), and CO-bound Zn-qNOR (g), ^{13}CO-bound Zn-qNOR (h), and the difference (CO − ^{13}CO) (i) at pH 9.0. Frequencies represent the peak positions detected in the CO − ^{13}CO difference spectra. The frequencies of ν_{Fe-CO} and ν_{C-O} are summarized in Table 1.

4. Discussion

In the present study, we report on some differences in the functional and structural properties of *G. stearothermophilus* qNOR compared to those of *P. aeruginosa* cNOR, as evidenced by biochemical and spectroscopic measurements. This makes it possible to delineate structure–function relationships in both cNOR and qNOR in the solution state, and discuss the possible functional differences between the two enzymes in relation to the structural differences observed in this study together with the crystal structures.

Our crystal structure of qNOR from *G. stearothermophilus* provided two unexpected structural findings: one being the dissociation of conserved Glu, Glu512, which has been shown by mutational study to be essential for the enzymatic activity, from the non-heme metal, and the other being the presence of a water channel from the cytoplasmic side to the active center [21]; neither of which was observed in *P. aeruginosa* cNOR, as shown in Fig. 5. Due to the dissociation of Glu512 from Zn_B, the carboxylate group of Glu512 in qNOR is located ~7 Å from the heme b_3 iron whereas, in the case of cNOR, the corresponding carboxylate group coordinates to non-heme iron and is located ~4 Å from the heme b_3 iron. Such a positional difference in conserved Glu between qNOR and cNOR could generate an active site with an entirely different environment. However, the dissociation of the Glu ligand in qNOR from the non-heme metal could be caused by the accidental replacement of non-heme Fe_B with Zn_B prior to crystallization. There is no evidence yet for likewise dissociation of the Glu ligand in the Fe_B-qNOR. Mononuclear non-heme iron proteins usually have one

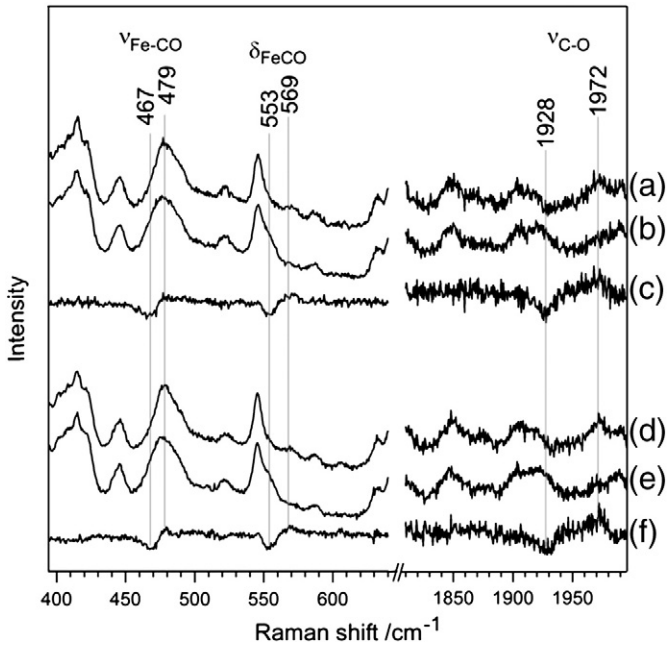

Fig. 4. Resonance Raman spectra of the reduced CO-bound cNOR from *P. aeruginosa* with excitation at 413.1 nm. Traces shown were obtained from CO-bound cNOR (a), ^{13}CO-bound cNOR (b), and the difference (CO − ^{13}CO) (c) at pH 9.0, and those at pH 6.0; (d), (e) and (f). Frequencies represent the peak positions detected in the CO − ^{13}CO difference spectra. The frequencies of ν_{Fe-CO} and ν_{C-O} are summarized in Table 1.

Table 1
Fe–CO and C–O stretching frequencies in NORs and CcOs.

Protein	Non-heme metal	ν_{Fe-CO} (cm^{-1})	ν_{C-O} (cm^{-1})	Ref.
G.s. qNOR[a]	Fe/Zn[g]	481/495	1962	This study
G.s. qNOR[a]	Zn[h]	481/525[i]	1962	This study
P.a. cNOR[b]	Fe	477	1972	This study
Pa.d. cNOR[c]	Fe	476	1970	[34]
Py.a. qNOR[d]	Fe	481	N.R.[j]	[22]
R.d. cNOR-homologue[e]	Cu	523	1969	[40]
Bovine aa_3 CcO	Cu	520	1963	[41]
R.s. aa_3 CcO[f]	Cu	519	1966	[41]
E. coli bo CcO	Cu	523	1960	[41]

[a] *G. stearothermophilus* qNOR.
[b] *P. aeruginosa* cNOR.
[c] *Pa. denitrificans* cNOR.
[d] *Py. aerophilum* qNOR.
[e] *R. denitrificans* cNOR-homologue.
[f] *Rhodobacter sphaeroides* aa_3 CcO.
[g] Fe and Zn occupy the non-heme metal site in qNOR prepared with DDM.
[h] Only Zn is present at the non-heme site in qNOR prepared with OG.
[i] The ν_{Fe-CO} at 525 cm^{-1} is the minor species.
[j] Not reported.

carboxylate, and two or three His imidazoles as ligands [35,36]. Since the coordination of one carboxylate is a very common feature of the active site architecture in non-heme iron proteins, we herewith adopt (assume) the same coordination structure for Fe_B in Fe_B-qNOR as that in cNOR.

With respect to the presence of the water channel, one might feel that the Zn_B substitution is the structural reason for the appearance of the water channel from the cytoplasmic side to the active center in *G. stearothermophilus* qNOR. However, in the alignment of primary sequences of qNORs, we found that the type of residues involved in the water channel in *G. stearothermophilus* qNOR is well conserved, as shown in Fig. 6. Therefore, in this study, we assume that the water channel is likely to be present, even in active Fe_B-qNOR. Indeed, our earlier work on a structure-based molecular dynamics simulation showed that Glu512 is associated with the non-heme metal without the water channel collapsing in the snapshot during the simulation [21], suggesting that the water channel may also be present in the Fe_B-qNOR, in which Glu512 can be a ligand for Fe_B.

4.1. Structural difference in the active site of *G. stearothermophilus* qNOR and *P. aeruginosa* cNOR

The frequencies of the ν_{Fe-CO} and ν_{C-O} modes in the vibration spectra are rich in information for deducing the environments of the binuclear active center of NORs. Fig. 6 displays a well-known ν_{Fe-CO} versus ν_{C-O} correlation plot [32,33] with the current data for the NORs. Due to heme-Fe $d_\pi \rightarrow CO\ \pi^*$ back-donation, the ν_{Fe-CO} and ν_{C-O} frequencies show a linear correlation with a negative slope [32,33]. For example, a negative environment and/or no hydrogen bonding interactions with the CO ligand decreases the back-donation from heme-Fe, leading to a lower ν_{Fe-CO} and a higher ν_{C-O}. In the case of *P. aeruginosa* cNOR, the data point is located at the lower end of the ν_{Fe-CO} (Fig. 7), which bears similarity to the data for the *Pa. denitrificans* cNOR [34]. As suggested in the study on *Pa. denitrificans* cNOR, the frequencies of ν_{Fe-CO} and ν_{C-O} in cNORs indicate that back-donation from the heme-Fe is minimized, likely because of a negatively charged distal pocket of heme b_3. On the basis of the crystal structure of *P. aeruginosa* cNOR, it

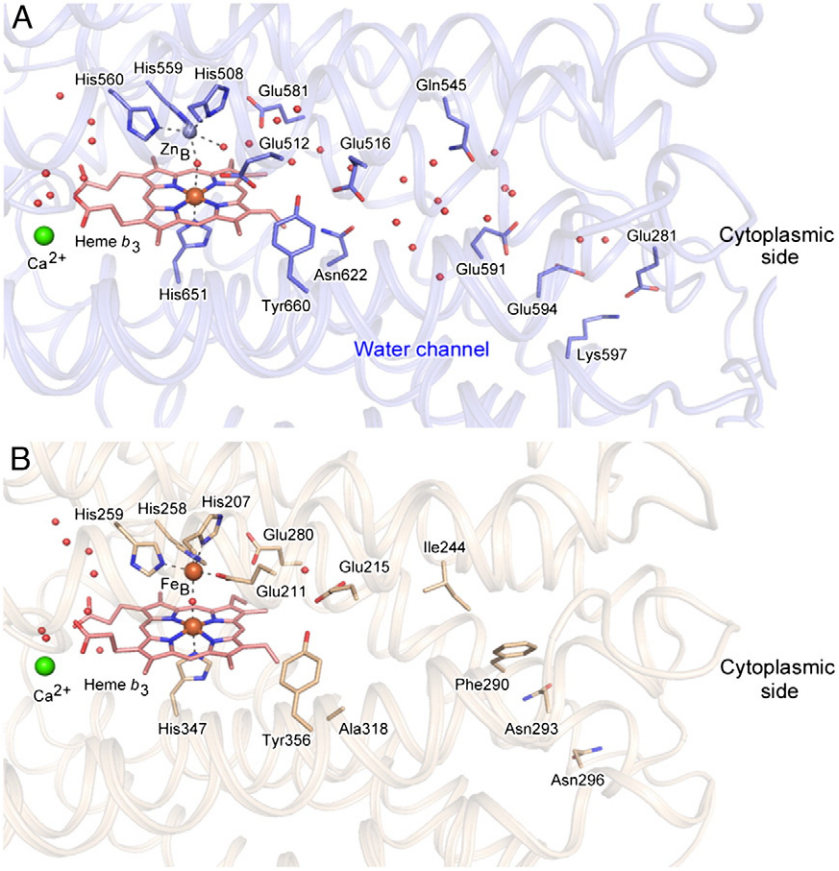

Fig. 5. Structures of the active site and the water channel regions in *G. stearothermophilus* qNOR (A) and *P. aeruginosa* cNOR (B). In *G. stearothermophilus* qNOR, conserved Glu512 is not a ligand for non-heme Zn_B, and a water channel from the cytoplasmic side is present. On the other hand, the conserved Glu211 is a ligand for non-heme Fe_B and the water channel is absent in *P. aeruginosa* cNOR.

		281	512 516	545	581	591 594 597	622	660
G.s.	qNOR	-MQ**E**AY-	-WV**E**GIF**E**VF-	-YF**Q**FT-	-AL**E**VI-	-IL**E**AY**E**QY**K**MM-	-IW**N**LV-	-GV**Y**GM-
S.a.	qNOR	-MK**P**TY-	-WV**E**GIF**E**AF-	-YF**Q**LT-	-AL**E**VV-	-IW**E**AY**T**HY**R**LY-	-LW**N**AI-	-GV**Y**GM-
C.m.	qNOR	-EE**P**LP-	-WV**E**GFF**E**VF-	-LA**S**AS-	-AL**E**VV-	-GE**E**AW**E**NW**R**LK-	-FW**N**ML-	-GV**Y**GF-
N.g.	qNOR	-EE--V-	-WV**E**GFF**E**VF-	-LA**A**AA-	-AL**E**VV-	-GR**E**AY**E**HW**S**YQ-	-FW**N**MI-	-GV**Y**GF-
S.	qNOR	-EE--V-	-WV**E**GFF**E**VF-	-YL**T**TI-	-AL**E**VV-	-GF**E**VV**K**SL**K**LS-	-VW**N**LV-	-GV**Y**GS-
M.c.	qNOR	-EE**D**DI-	-WV**E**GFF**E**VF-	-IA**S**AA-	-AL**E**VV-	-GY**E**GY**E**HW**S**MQ-	-VW**N**ML-	-GV**Y**GF-
A.x.	qNOR	-EE**D**---	-WV**E**GFF**E**VF-	-LA**S**AS-	-AL**E**VV-	-GH**E**AW**E**NW**R**LK-	-FW**N**ML-	-GV**Y**GF-
R.e.	qNOR	-EE**A**---	-WV**E**GFF**E**VF-	-LA**S**RS-	-AL**E**VV-	-GH**E**AW**D**NW**R**LK-	-FW**N**ML-	-GV**Y**GF-
C.d.	qNOR	-ED**E**IN-	-WV**E**GFF**E**VF-	-IS**S**TT-	-AL**E**VV-	-GI**E**AL**H**NL**R**LL-	-FW**N**MV-	-GV**Y**GM-
C.s.	qNOR	-EE----	-WV**E**GFF**E**VF-	-YL**T**TI-	-AL**E**VV-	-GF**E**VL**K**SM**R**LS-	-FW**N**LI-	-GV**Y**GS-

Fig. 6. Sequence alignments of the amino acid residues located at the water channel in qNOR. Sequence data are from the EMBL and NCBI databases. The alignment was produced from ~350 of qNOR sequences by ClustalX [39]. From the alignment, Glu512 is fully conserved; Glu516 is well-conserved (97%), Gln545 is not conserved (20% Gln, 25% Ser, 20% Asp, 15% Ala, 12% Glu, 7% Thr), but balky hydrophobic residues are not observed at this position, Glu581 is fully conserved, Glu591 is well-conserved (88% Glu, 7% Asp), Glu594 is not conserved (36% Glu, 17% Gly, 11% His, 7% Asp, 7% Lys, 6% Ala, 5% Thr), but balky hydrophobic residues are not observed at this position, Lys597 is not fully conserved (50% Arg, 15% Lys, 18% Gln, 11% Ser), but positive charge is highly conserved, Asn622 is well-conserved (97%), and Tyr660 is highly conserved (75% Tyr, 25% Phe). The alignment of position at 281 is difficult, since Glu281 is located at a loop region. Ten selected sequences of qNOR from different bacteria, *G.s.*, *G. stearothermophilus*; *S.a.*, *Staphylococcus aureus*; *C.m.*, *Cupriavidus metallidurans*; *N.g.*, *Neisseria gonorrhoeae*; *S.*, *Synechocystis* sp. PCC 6803; *M.c.*, *Moraxella catarrhalis*; *A.x.*, *Achromobacter xylosoxidans*; *R.e.*, *Ralstonia eutropha*; *C.d.*, *Corynebacterium diphtheriae* and *C.s.*, *Cyanobacterium stanieri* are shown here.

is plausible that the three conserved Glu residues, Glu211, Glu215 and Glu280, create a negative environment for the CO ligand.

To gain insights into the structure–function relationships of qNOR, we focused on the active form of qNOR, Fe_B-qNOR. Fe_B-qNOR exhibits a higher ν_{Fe-CO} (495 cm^{-1}) and a lower ν_{C-O} (1962 cm^{-1}) than those of cNOR (ν_{Fe-CO}: 478 cm^{-1} and ν_{C-O}: 1970 cm^{-1}), indicating that the back-donation from heme-Fe to the CO ligand in qNOR is weaker. The binuclear center of qNOR would, therefore, be a less negative and/or a more polar environment, as compared with the cNOR. Given that qNOR, similar to cNOR, has three conserved Glu, Glu512, Glu516 and Glu581, near the active site, it is likely that the active site of qNOR is also a highly negative environment, and that the structural difference may arise from the different polarity between the two NORs. One possible reason for the environmental difference in qNOR and cNOR would be the presence of the unique water channel that connects the binuclear center with the cytoplasm in qNOR (Fig. 5). The presence of the water channel facilitates the access of solvent water molecules to the active site, which creates a more polar environment at the active site in qNOR, thereby resulting in a higher ν_{Fe-CO} and a lower ν_{C-O} than the corresponding values for cNOR.

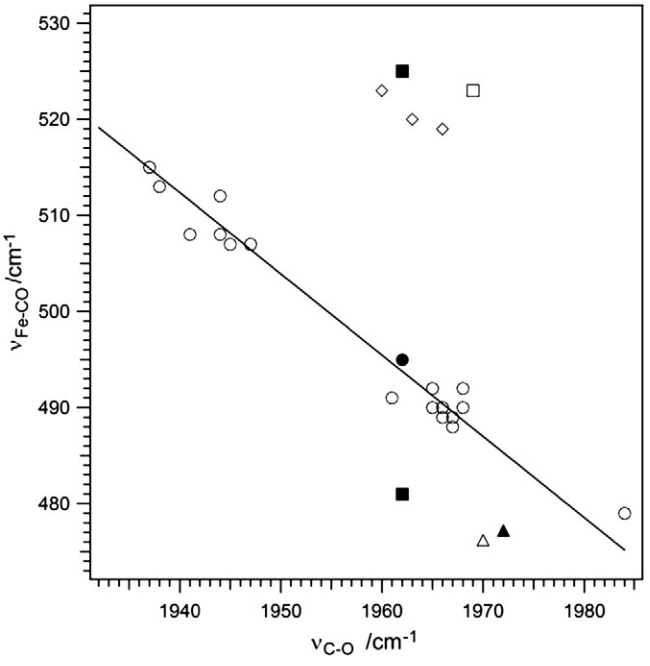

Fig. 7. ν_{Fe-CO} versus ν_{C-O} correlation plot of hemeproteins with axial histidine ligand. The solid curve represents a negative correlation between ν_{Fe-CO} and ν_{C-O} for general histidine-ligated hemeproteins (*open circles*) such as myoglobin [33]. The other plots show data for Fe_B-qNOR from *G. stearothermophilus* by *closed circle*, Zn_B-qNOR from *G. stearothermophilus* by *closed squares*, cNOR form *P. aeruginosa* by *closed triangle*, cNOR from *Pa. denitrificans* by *open triangle* [34], *Roseobacter denitrificans* by *open square* [40], and CcOs by *open diamonds* [41].

4.2. Origin of different functional properties in G. stearothermophilus qNOR and P. aeruginosa cNOR

In addition to the structural difference between the two types of NORs, biochemical analyses indicate that the reduction of qNOR was much slower than that for cNOR, and implies that qNOR has a lower redox potential compared to cNOR. Our finding of a more polar environment at the active site of qNOR likely enhances the interaction of the ferric iron with the water dipoles, which could explain the lower redox potential of qNOR compared to cNOR. In fact, a lowered redox potential upon increase in accessibility of the redox center to solvent water molecules has been reported for other metalloproteins. For example, one particular mutant of blue-copper azurin enhances the accessibility of the Cu center to solvent by opening of the cavity, which then becomes filled with water molecules in the vicinity of the Cu center, and shows a negative shift in redox potential compared to the wild-type protein [37,38]. Thus, the water channel that is not observed in the cNOR could be a key factor in controlling the properties of the active site, such as the redox potential, in qNOR, which results in having different functional properties from that of cNOR.

If the presence of the water channel is a common structural feature in qNOR, it is possible that qNOR would have a polar environment at the active site and possibly a lower redox potential as compared with cNOR. The possibility of a more polar active site in qNOR is supported by a previous spectroscopic study on qNOR from archaeon *Pyrobaculum aerophilum* [22]. In a resonance Raman study on qNOR from *Py. aerophilum*, the ν_{Fe-CO} peak was observed at 481 cm^{-1}, though, unfortunately, the ν_{C-O} could not be determined [22]. Similar to *G. stearothermophilus* qNOR, a higher ν_{Fe-CO} peak (481 cm^{-1}) than that of cNOR (477 cm^{-1}) suggests the existence of a more polar environment at the binuclear center in *Py. aerophilum* qNOR. In addition, a more negative redox potential in qNOR relative to that of cNOR is functionally reasonable, since the physiological reductant for qNOR, menaquinone, has a lower redox potential ($E_m = -74$ mV) than that of cytochrome c_{551} ($E_m =$ 240–260 mV) which supplies electrons to cNOR in vivo. Although more structural and functional studies on qNORs will clearly be needed to reach a firm conclusion, the environment of the active site in qNOR appears to be more polar than that of cNOR.

The findings reported herein indicate that *G. stearothermophilus* qNOR clearly has different functional properties from those of *P. aeruginosa* cNOR. A close examination of the binuclear active center based on resonance Raman measurements revealed that qNOR appears to have a

more polar environment at the binuclear center as compared with cNOR. On the basis of the current findings along with the crystal structures, we propose that a water channel from the cytoplasm to the active site is present and that this results in a more polar environment at the active site in qNOR. Such structural characteristics might result in different active site properties, such as the redox potential, thus leading to differing functional properties for the two NORs. We are currently characterizing the structure and function of qNORs from the other bacterial sources, in particular pathogenic bacteria. Information regarding these qNORs should help us to develop a better understanding of the common structural and functional aspects on qNOR, which will then allow us to further elucidate the catalytic mechanism for the NO reduction reaction and the molecular evolution of the respiratory enzymes.

Acknowledgements

We thank K. Takatsu (RIKEN) for support in the preparation of qNOR and cNOR, and D. Young (RIKEN and Univ. of Liverpool) for the proof-reading. We also thank Prof. T. Ogura (Univ. of Hyogo) for kindly permitting us to use his Raman equipment. This work was supported by grants from the Ministry of Education, Culture, Sports, Science and Technology (22770136 to T.T., and 21245041 to Y.S.).

References

[1] A.R. Ravishankara, J.S. Daniel, R.W. Portmann, Nitrous oxide (N_2O): the dominant ozone-depleting substance emitted in the 21st century, Science 326 (2009) 123–125.
[2] M. Saraste, J. Castresana, Cytochrome oxidase evolved by tinkering with denitrification enzymes, FEBS Lett. 341 (1994) 1–4.
[3] F.L. Sousa, R.J. Alves, M.A. Ribeiro, J.B. Pereira-Leal, M. Teixeira, M.M. Pereira, The superfamily of heme–copper oxygen reductases: types and evolutionary considerations, Biochim. Biophys. Acta 1817 (2012) 629–637.
[4] J. van der Oost, A.P. de Boer, J.W. de Gier, W.G. Zumft, A.H. Stouthamer, R.J. van Spanning, The heme–copper oxidase family consists of three distinct types of terminal oxidases and is related to nitric oxide reductase, FEMS Microbiol. Lett. 121 (1994) 1–9.
[5] S. Ferguson-Miller, C. Hiser, J. Liu, Gating and regulation of the cytochrome *c* oxidase proton pump, Biochim. Biophys. Acta 1817 (2012) 489–494.
[6] S. Yoshikawa, K. Muramoto, K. Shinzawa-Itoh, The O_2 reduction and proton pumping gate mechanism of bovine heart cytochrome *c* oxidase, Biochim. Biophys. Acta 1807 (2011) 1279–1286.
[7] S. Yoshikawa, K. Muramoto, K. Shinzawa-Itoh, H. Aoyama, T. Tsukihara, K. Shimokata, Y. Katayama, H. Shimada, Proton pumping mechanism of bovine heart cytochrome *c* oxidase, Biochim. Biophys. Acta 1757 (2006) 1110–1116.
[8] W.G. Zumft, Nitric oxide reductases of prokaryotes with emphasis on the respiratory, heme–copper oxidase type, J. Inorg. Biochem. 99 (2005) 194–215.
[9] J. Hendriks, A. Oubrie, J. Castresana, A. Urbani, S. Gemeinhardt, M. Saraste, Nitric oxide reductases in bacteria, Biochim. Biophys. Acta 1459 (2000) 266–273.
[10] S. de Vries, I. Schroder, Comparison between the nitric oxide reductase family and its aerobic relatives, the cytochrome oxidases, Biochem. Soc. Trans. 30 (2002) 662–667.
[11] T.M. Stevanin, J.W. Moir, R.C. Read, Nitric oxide detoxification systems enhance survival of *Neisseria meningitidis* in human macrophages and in nasopharyngeal mucosa, Infect. Immun. 73 (2005) 3322–3329.
[12] K. Kakishima, A. Shiratsuchi, A. Taoka, Y. Nakanishi, Y. Fukumori, Participation of nitric oxide reductase in survival of *Pseudomonas aeruginosa* in LPS-activated macrophages, Biochem. Biophys. Res. Commun. 355 (2007) 587–591.
[13] M.J. Strampraad Suharti, I. Schroder, S. de Vries, A novel copper A containing menaquinol NO reductase from *Bacillus azotoformans*, Biochemistry 40 (2001) 2632–2639.
[14] P. Moënne-Loccoz, Spectroscopic characterization of heme iron–nitrosyl species and their role in NO reductase mechanisms in diiron proteins, Nat. Prod. Rep. 24 (2007) 610–620.
[15] H. Kumita, K. Matsuura, T. Hino, S. Takahashi, H. Hori, Y. Fukumori, I. Morishima, Y. Shiro, NO reduction by nitric-oxide reductase from denitrifying bacterium *Pseudomonas aeruginosa*: characterization of reaction intermediates that appear in the single turnover cycle, J. Biol. Chem. 279 (2004) 55247–55254.
[16] M.R. Blomberg, P.E. Siegbahn, Mechanism for N_2O generation in bacterial nitric oxide reductase: a quantum chemical study, Biochemistry 51 (2012) 5173–5186.
[17] J. Reimann, U. Flock, H. Lepp, A. Honigmann, P. Ädelroth, A pathway for protons in nitric oxide reductase from *Paracoccus denitrificans*, Biochim. Biophys. Acta 1767 (2007) 362–373.
[18] T. Hino, Y. Matsumoto, S. Nagano, H. Sugimoto, Y. Fukumori, T. Murata, S. Iwata, Y. Shiro, Structural basis of biological N_2O generation by bacterial nitric oxide reductase, Science 330 (2010) 1666–1670.
[19] A.V. Pisliakov, T. Hino, Y. Shiro, Y. Sugita, Molecular dynamics simulations reveal proton transfer pathways in cytochrome C-dependent nitric oxide reductase, PLoS Comput. Biol. 8 (2012) e1002674.
[20] J.P. Shapleigh, W.J. Payne, Nitric oxide-dependent proton translocation in various denitrifiers, J. Bacteriol. 163 (1985) 837–840.
[21] Y. Matsumoto, T. Tosha, A.V. Pisliakov, T. Hino, H. Sugimoto, S. Nagano, Y. Sugita, Y. Shiro, Crystal structure of quinol-dependent nitric oxide reductase from *Geobacillus stearothermophilus*, Nat. Struct. Mol. Biol. 19 (2012) 238–245.
[22] S. de Vries, M.J. Strampraad, S. Lu, P. Moënne-Loccoz, I. Schroder, Purification and characterization of the MQH_2:NO oxidoreductase from the hyperthermophilic archaeon *Pyrobaculum aerophilum*, J. Biol. Chem. 278 (2003) 35861–35868.
[23] R. Cramm, A. Pohlmann, B. Friedrich, Purification and characterization of the single-component nitric oxide reductase from *Ralstonia eutropha* H16, FEBS Lett. 460 (1999) 6–10.
[24] L. Salomonsson, J. Reimann, T. Tosha, N. Krause, N. Gonska, Y. Shiro, P. Ädelroth, Proton transfer in the quinol-dependent nitric oxide reductase from *Geobacillus stearothermophilus* during reduction of oxygen, Biochim. Biophys. Acta 1817 (2012) 1914–1920.
[25] P. Girsch, S. de Vries, Purification and initial kinetic and spectroscopic characterization of NO reductase from *Paracoccus denitrificans*, Biochim. Biophys. Acta 1318 (1997) 202–216.
[26] T.N. Nazina, T.P. Tourova, A.B. Poltaraus, E.V. Novikova, A.A. Grigoryan, A.E. Ivanova, A.M. Lysenko, V.V. Petrunyaka, G.A. Osipov, S.S. Belyaev, M.V. Ivanov, Taxonomic study of aerobic thermophilic bacilli: descriptions of *Geobacillus subterraneus* gen. nov., sp. nov. and *Geobacillus uzenensis* sp. nov. from petroleum reservoirs and transfer of *Bacillus stearothermophilus*, *Bacillus thermocatenulatus*, *Bacillus thermoleovorans*, *Bacillus kaustophilus*, *Bacillus thermoglucosidasius* and *Bacillus thermodenitrificans* to *Geobacillus* as the new combinations *G. stearothermophilus*, *G. thermocatenulatus*, *G. thermoleovorans*, *G. kaustophilus*, *G. thermoglucosidasius* and *G. thermodenitrificans*, Int. J. Syst. Evol. Microbiol. 51 (2001) 433–446.
[27] L.A. Schurig-Briccio, P. Venkatakrishnan, J. Hemp, C. Bricio, J. Berenguer, R.B. Gennis, Characterization of the nitric oxide reductase from *Thermus thermophilus*, Proc. Natl. Acad. Sci. U. S. A. 110 (2013) 12613–12618.
[28] K.L. Gronberg, M.D. Roldan, L. Prior, G. Butland, M.R. Cheesman, D.J. Richardson, S. Spiro, A.J. Thomson, N.J. Watmough, A low-redox potential heme in the dinuclear center of bacterial nitric oxide reductase: implications for the evolution of energy-conserving heme–copper oxidases, Biochemistry 38 (1999) 13780–13786.
[29] J.H. Hendriks, A. Jasaitis, M. Saraste, M.I. Verkhovsky, Proton and electron pathways in the bacterial nitric oxide reductase, Biochemistry 41 (2002) 2331–2340.
[30] J.H. Hendriks, L. Prior, A.R. Baker, A.J. Thomson, M. Saraste, N.J. Watmough, Reaction of carbon monoxide with the reduced active site of bacterial nitric oxide reductase, Biochemistry 40 (2001) 13361–13369.
[31] U. Flock, N.J. Watmough, P. Ädelroth, Electron/proton coupling in bacterial nitric oxide reductase during reduction of oxygen, Biochemistry 44 (2005) 10711–10719.
[32] T. Uchida, T. Kitagawa, Mechanism for transduction of the ligand-binding signal in heme-based gas sensory proteins revealed by resonance Raman spectroscopy, Acc. Chem. Res. 38 (2005) 662–670.
[33] T.G. Spiro, I.H. Wasbotten, CO as a vibrational probe of heme protein active sites, J. Inorg. Biochem. 99 (2005) 34–44.
[34] P. Moënne-Loccoz, S. de Vries, Structural characterization of the catalytic high-spin heme *b* of nitric oxide reductase: a resonance Raman study, J. Am. Chem. Soc. 120 (1998) 5147–5152.
[35] M.M. Abu-Omar, A. Loaiza, N. Hontzeas, Reaction mechanisms of mononuclear non-heme iron oxygenases, Chem. Rev. 105 (2005) 2227–2252.
[36] M.S. Lah, M.M. Dixon, K.A. Pattridge, W.C. Stallings, J.A. Fee, M.L. Ludwig, Structure–function in *Escherichia coli* iron superoxide dismutase: comparisons with the manganese enzyme from *Thermus thermophilus*, Biochemistry 34 (1995) 1646–1660.
[37] G. Battistuzzi, M. Borsari, G.W. Canters, E. de Waal, L. Loschi, G. Warmerdam, M. Sola, Enthalpic and entropic contributions to the mutational changes in the reduction potential of azurin, Biochemistry 40 (2001) 6707–6712.
[38] H. Nar, A. Messerschmidt, R. Huber, M. van de Kamp, G.W. Canters, X-ray crystal structure of the two site-specific mutants His35Gln and His35Leu of azurin from *Pseudomonas aeruginosa*, J. Mol. Biol. 218 (1991) 427–447.
[39] M.A. Larkin, G. Blackshields, N.P. Brown, R. Chenna, P.A. McGettigan, H. McWilliam, F. Valentin, I.M. Wallace, A. Wilm, R. Lopez, J.D. Thompson, T.J. Gibson, D.G. Higgins, Clustal W and Clustal X version 2.0, Bioinformatics 23 (2007) 2947–2948.
[40] Y. Matsuda, T. Uchida, H. Hori, T. Kitagawa, H. Arata, Structural characterization of a binuclear center of a Cu-containing NO reductase homologue from *Roseobacter denitrificans*: EPR and resonance Raman studies, Biochim. Biophys. Acta 1656 (2004) 37–45.
[41] M. Tsubaki, K. Matsushita, O. Adachi, S. Hirota, T. Kitagawa, H. Hori, Resonance Raman, infrared, and EPR investigation on the binuclear site structure of the heme–copper ubiquinol oxidases from *Acetobacter aceti*: effect of the heme peripheral formyl group substitution, Biochemistry 36 (1997) 13034–13042.